

f -GAIL: Learning f -Divergence for Generative Adversarial Imitation Learning

Xin Zhang[†], Yanhua Li[†], Ziming Zhang[†], Zhi-Li Zhang[§]
 Worcester Polytechnic Institute, USA[†], University of Minnesota, USA[§]
 {xzhang17, yli15, zzhang15}@wpi.edu, zhzhzhang@cs.umn.edu

Abstract

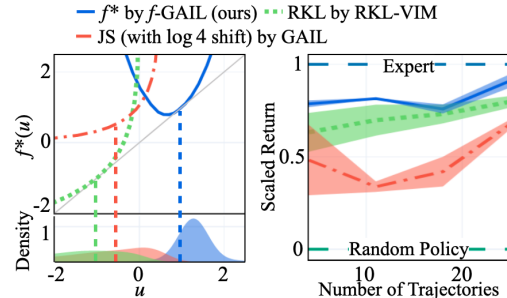
Imitation learning (IL) aims to learn a policy from expert demonstrations that minimizes the discrepancy between the learner and expert behaviors. Various imitation learning algorithms have been proposed with different *pre-determined* divergences to quantify the discrepancy. This naturally gives rise to the following question: *Given a set of expert demonstrations, which divergence can recover the expert policy more accurately with higher data efficiency?* In this work, we propose f -GAIL, a new generative adversarial imitation learning (GAIL) model, that automatically learns a discrepancy measure from the f -divergence family as well as a policy capable of producing expert-like behaviors. Compared with IL baselines with various predefined divergence measures, f -GAIL learns better policies with higher data efficiency in six physics-based control tasks.

1 Introduction

Imitation Learning (IL) or Learning from Demonstrations (LfD) [1, 6, 18] aims to learn a policy directly from expert demonstrations, without access to the environment for more data or any reward signal. One successful IL paradigm is Generative Adversarial Imitation Learning (GAIL) [18], which employs generative adversarial network (GAN) [15] to jointly learn a generator (as a stochastic policy) to mimic expert behaviors, and a discriminator (as a reward signal) to distinguish the generated vs expert behaviors. The learned policy produces behaviors similar to the expert, and the similarity is evaluated using the reward signal, in Jensen-Shannon (JS) divergence (with a constant shift of $\log 4$ [24]) between the distributions of learner vs expert behaviors. Thus, GAIL can be viewed as a variational divergence minimization (VDM) [25] problem with JS-divergence as the objective.

Beyond JS-divergence (as originally employed in GAIL), variations of GAIL have been proposed [18, 13, 12, 20, 14], essentially using different divergence measures from the f -divergence family [24, 25], for example, behavioral cloning (BC) [26] with Kullback-Leibler (KL) divergence [24], AIRL [13] and RKL-VIM [20] with reverse KL (RKL) divergence [24], and DAGGER [28] with the Total Variation (TV) [7]. Choosing the right divergence is crucial in order to recover the expert policy more accurately with high data efficiency (as observed in [20, 14, 18, 13, 25, 33]).

Motivation. All the above literature works rely on a *fixed* divergence measure manually chosen *a priori* from a set of well-known divergence measures (with an explicit analytic form), e.g., KL, RKL, JS, ignoring the large space of all potential



(a) f^* of f -divergence. (b) Return of learned policies.

Figure 1: f -divergences and policies from GAIL, RKL-VIM, and f -GAIL on Walker task [32].

divergences. Thus, the resulting IL network likely learns a sub-optimal learner policy. For example, Fig. 1 shows the results from GAIL [18] and RKL-VIM [20], which employ JS and RKL divergences, respectively. The learned input density distributions (to the divergence functions) are quite dispersed (thus with large overall divergence) in Fig. 1(a), leading to learner policies with only 30%-70% expert return in Fig. 1(b). In this work, we are motivated to develop a *learnable* model to search and automatically find an appropriate discrepancy measure from the f -divergence family for GAIL.

Our f -GAIL. We propose f -GAIL – a new generative adversarial imitation learning model, with a *learnable* f -divergence from the underlying expert demonstrations. The model automatically learns an f -divergence between expert and learner behaviors, and a policy that produces expert-like behaviors. In particular, we propose a deep neural network structure to model the f -divergence space. Fig. 1 shows a quick view of our results: f -GAIL learns a new and unique f -divergence, with more concentrated input density distribution (thus smaller overall divergence) than JS and RKL in Fig. 1(a); and its learner policy has higher performance (80%-95% expert return) in Fig. 1(b) (See more details in Sec 4). The code for reproducing the experiments are available at <https://github.com/fGAIL3456/fGAIL>. Our key contributions are summarized below:

- We are the *first* to model imitation learning with a ***learnable divergence measure*** from f -divergence space, which yields better learner policies, than pre-defined divergence choices (Sec 2).
- We develop an f^* -network structure, to model the space of f -divergence family, by enforcing two constraints, including i) convexity and ii) $f(1) = 0$ (Sec 3).
- We present promising comparison results of learned f -divergences and the performances of learned policies with baselines in six different physics-based control tasks (Sec 4).

2 Problem Definition

2.1 Preliminaries

Markov Decision Processes (MDPs). In an MDP denoted as a 6-tuple $\langle \mathcal{S}, \mathcal{A}, \mathcal{P}, r, \rho_0, \gamma \rangle$ where \mathcal{S} is a set of states, \mathcal{A} is a set of actions, $\mathcal{P} : \mathcal{S} \times \mathcal{A} \times \mathcal{S} \mapsto [0, 1]$ is the transition probability distribution, $r : \mathcal{S} \times \mathcal{A} \mapsto \mathbb{R}$ is the reward function, $\rho_0 : \mathcal{S} \mapsto \mathbb{R}$ is the distribution of the initial state s_0 , and $\gamma \in [0, 1]$ is the discount factor. We denote the expert policy as π_E , and the learner policy as π . In addition, we use an expectation with respect to a policy π to denote an expectation with respect to the trajectories it generates: $\mathbb{E}_\pi[h(s, a)] \triangleq \mathbb{E}[\sum_{t=0}^{\infty} \gamma^t h(s_t, a_t)]$, with $s_0 \sim \rho_0, a_t \sim \pi(a_t|s_t), s_{t+1} \sim \mathcal{P}(s_{t+1}|s_t, a_t)$ and h as any function.

f -Divergence. f -Divergence [24, 23, 11] is a broad class of divergences that measures the difference between two probability distributions. Different choices of f functions recover different divergences, e.g. the Kullback-Leibler (KL) divergence, Jensen-Shannon (JS) divergence, or total variation (TV) distance [22]. Given two distributions P and Q , an absolutely continuous density function $p(x)$ and $q(x)$ over a finite set of random variables x defined on the domain \mathcal{X} , an f -divergence is defined as

$$D_f(P\|Q) = \int_{\mathcal{X}} q(x) f\left(\frac{p(x)}{q(x)}\right) dx, \quad (1)$$

with the generator function $f : \mathbb{R}_+ \rightarrow \mathbb{R}$ as a convex, lower-semicontinuous function satisfying $f(1) = 0$. The *convex conjugate* function f^* also known as the *Fenchel conjugate* [16] is $f^*(u) = \sup_{v \in \text{dom}_f} \{vu - f(v)\}$. $D_f(P\|Q)$ is lower bounded by its variational transformation, i.e., $D_f(P\|Q) \geq \sup_{u \in \text{dom}_{f^*}} \{\mathbb{E}_{x \sim P}[u] - \mathbb{E}_{x \sim Q}[f^*(u)]\}$ (See more details in [25]). Common choices of f functions are summarized in Tab. 1 and the plots of corresponding f^* are visualized in Fig. 4.

Imitation Learning as Variational f -Divergence Minimization (VDM). Imitation learning aims to learn a policy for performing a task directly from expert demonstrations. GAIL [18] is an IL solution employing GAN [15] structure, that jointly learns a generator (i.e., learner policy) and a discriminator (i.e., reward signal). In the training process of GAIL, the learner policy imitates the behaviors from the expert policy π_E , to match the generated state-action distribution with that of the expert. The distance between these two distributions, measured by JS divergence, is minimized. Thus the GAIL objective is stated as follows:

$$\min_{\pi} \max_T \mathbb{E}_{\pi_E}[\log T(s, a)] + \mathbb{E}_{\pi}[\log(1 - T(s, a))] - \mathcal{H}(\pi), \quad (2)$$

where T is a binary classifier distinguishing state-action pairs generated by π vs π_E , and it can be viewed as a reward signal used to guide the training of policy π . $\mathcal{H}(\pi) = \mathbb{E}_\pi[-\log \pi(a|s)]$ is the γ -discounted causal entropy of the policy π [18]. Using the variational lower bound of an f -divergence, several studies [20, 14, 25, 5] have extended GAIL to a general variational f -divergence minimization (VDM) problem for a fixed f -divergence (defined by a generator function f), with an objective below,

$$\min_{\pi} \max_T \mathbb{E}_{\pi_E}[T(s, a)] - \mathbb{E}_{\pi}[f^*(T(s, a))] - \mathcal{H}(\pi). \quad (3)$$

However, all these works rely on manually choosing an f -divergence measure, i.e., f^* , which is limited by those well-known f -divergence choices (ignoring the large space of all potential f -divergences), thus lead to a sub-optimal learner policy. Hence, we are motivated to develop a new and more general GAIL model, which automatically searches an f -divergence from the f -divergence space given expert demonstrations.

2.2 Problem Definition: Imitation Learning with Learnable f -Divergence.

Divergence Choice Matters! As observed in [20, 14, 13, 25, 33], given an imitation learning task, defined by a set of expert demonstrations, different divergence choices lead to different learner policies. Taking KL divergence and RKL divergence (defined in eq. (4) below) as an example, let $p(x)$ be the true distribution, and $q(x)$ be the approximate distribution learned by minimizing its divergence from $p(x)$. With KL divergence, the difference between $p(x)$ and $q(x)$ is weighted by $p(x)$. Thus, in the ranges of x with $p(x) = 0$, the discrepancy of $q(x) > 0$ from $p(x)$ will be ignored. On the other hand, with RKL divergence, $q(x)$ becomes the weight. In the ranges of x with $q(x) = 0$, RKL divergence does not capture the discrepancy of $q(x)$ from $p(x) > 0$. Hence, KL divergence can be used to better learn multiple modes from a true distribution $p(x)$ (i.e., for mode-covering), while RKL divergence will perform better in learning a single mode (i.e., for mode-seeking).

$$D_{KL}(P\|Q) = \int_{\mathcal{X}} p(x) \log \left(\frac{p(x)}{q(x)} \right) dx, \quad D_{RKL}(P\|Q) = \int_{\mathcal{X}} q(x) \log \left(\frac{q(x)}{p(x)} \right) dx. \quad (4)$$

Beyond KL and RKL divergences, there are infinitely many choices in the f -divergence family, where each divergence measures the discrepancy between expert vs learner distributions from a unique perspective. Hence, choosing the right divergence for an imitation learning task is crucial and can more accurately recover the expert policy with higher data efficiency.

f -GAIL: Imitation Learning with Learnable f -Divergence. Given a set of expert demonstrations to imitate and learn from, the f -divergence, that can highly evaluate the discrepancy between the learner and expert distributions (i.e., the largest f -divergence from the family), can better guide the learner to learn from the expert (as having larger improvement margin). As a result, in addition to the policy function π , the reward signal function T , we aim to learn a (convex conjugate) generator function f^* as a regularization term to the objective. The f -GAIL objective is as follows,

$$\min_{\pi} \max_{f^* \in \mathcal{F}^*, T} \mathbb{E}_{\pi_E}[T(s, a)] - \mathbb{E}_{\pi}[f^*(T(s, a))] - \mathcal{H}(\pi), \quad (5)$$

where \mathcal{F}^* denotes the admissible function space of f^* , namely, each function in \mathcal{F}^* represents a valid f -divergence. The conditions for a generator function f to represent an f -divergence include: i) convexity and ii) $f(1) = 0$. In other words, the corresponding convex conjugate f^* needs to be i) convex (**the convexity constraint**), ii) $\inf_{u \in \text{dom}_{f^*}} \{f^*(u) - u\} = 0$ (**the zero gap constraint**, namely, the minimum distance from $f^*(u)$ to u is 0)¹. Functions satisfying these two conditions form the admissible space \mathcal{F}^* . Note that the zero gap constraint can be obtained by combining convex conjugate $f(v) = \sup_{u \in \text{dom}_{f^*}} \{uv - f^*(u)\}$ and $f(1) = 0$. Tab. 1² below shows a comparison of our proposed f -GAIL with the state-of-the-art GAIL models [18, 13, 14, 20]. These models use pre-defined f -divergences, where f -GAIL can learn an f -divergence from f -divergence family.

Table 1: f -Divergence and imitation learning (JS* is a constant shift of JS divergence by $\log 4$).

Divergence	KL	RKL	JS*	Learned f -div.
$f^*(u)$	e^{u-1}	$-1 - \log(-u)$	$-\log(1 - e^u)$	$f^* \in \mathcal{F}^*$ from eq. (5)
IL Method	FAIRL[14]	RKL-VIM[20], AIRL[13]	GAIL[18]	f -GAIL (Ours)

¹Convex and zero-gap constraints are necessary and sufficient conditions to guarantee an f -divergence, based on $f^{**} = f$ (see §3.3.2 in [9]) for convex functions, i.e., $f(1) = f^{**}(1) = \max_u \{u - f^*(u)\} = 0$.

²Similar observations can be found in [20, 14].

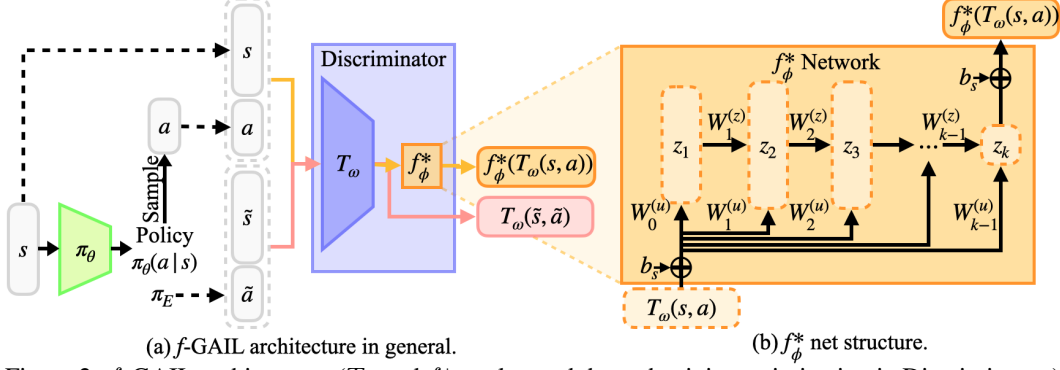


Figure 2: f -GAIL architecture. (T_ω and f_ϕ^* are learned through a joint optimization in Discriminator.)

3 Imitation Learning with Learnable f -Divergence

There are three functions to learn in the f -GAIL objective in eq. (5), including the policy π , the f^* -function f^* , and the reward signal T , where we model them with three deep neural networks parameterized by θ, ω and ϕ respectively. Following the generative-adversarial approach [15], f_ϕ^* and T_ω networks together can be viewed as a discriminator. The policy network π_θ is the generator. As a result, the goal is to find the saddle-point of the objective in eq. (5), where we minimize it with respect to θ and maximize it with respect to ω and ϕ . In this section, we will tackle two key challenges including i) how to design an algorithm to jointly learn all three networks to solve the f -GAIL problem in eq. (5)? (See Sec 3.1); and ii) how to design the f_ϕ^* network structure to enforce it to represent a valid f -divergence? (See Sec 3.2). Fig. 2 shows the overall f -GAIL model structure.

3.1 f -GAIL Algorithm

Our proposed f -GAIL algorithm is presented in Alg. 1. It uses the alternating gradient method (instead of one-step gradient method in f -GAN [25]) to first update the f^* -function f_ϕ^* and the reward signal T_ω in a single back-propagation, and then update the policy π_θ . It utilizes Adam [21] gradient step on ω to increase the objective in eq. (5) with respect to both T_ω and f_ϕ^* , followed by a shifting operation on f_ϕ^* to guarantee the zero gap constraint (See Sec 3.2 and eq. (7)). Then, it uses the Trust Region Policy Optimization (TRPO) [29] step on θ to decrease eq. (5) with respect to π_θ .

Algorithm 1 f -GAIL

Require: Initialize parameters of policy π_θ , reward signal T_ω , and f_ϕ^* networks as θ_0, ω_0 and ϕ_0 (with shifting operation eq. (7) required on ϕ_0 to enforce the zero gap constraint); expert trajectories $\tau_E \sim \pi_E$ containing state-action pairs.

Ensure: Learned policy π_θ , f^* -function f_ϕ^* and reward signal T_ω .

- 1: **for** each epoch $i = 0, 1, 2, \dots$ **do**
 - 2: Sample trajectories $\tau_i \sim \pi_{\theta_i}$.
 - 3: Sample state-action pairs: $\mathcal{D}_E \sim \tau_E$ and $\mathcal{D}_i \sim \tau_i$ with the same batch size.
 - 4: Update ω_i to ω_{i+1} and ϕ_i to ϕ_{i+1} by ascending with the gradients:

$$\Delta_{\omega_i} = \hat{\mathbb{E}}_{\mathcal{D}_E}[\nabla_{\omega_i} T_{\omega_i}(s, a)] - \hat{\mathbb{E}}_{\mathcal{D}_i}[\nabla_{\omega_i} f_{\phi_i}^*(T_{\omega_i}(s, a))], \quad \Delta_{\phi_i} = -\hat{\mathbb{E}}_{\mathcal{D}_i}[\nabla_{\phi_i} f_{\phi_i}^*(T_{\omega_i}(s, a))].$$
 - 5: Estimate the minimum gap δ with gradient descent in Alg. 2 and shift $f_{\phi_{i+1}}^*$ (by eq. (7)).
 - 6: Take a policy step from θ_i to θ_{i+1} , using the TRPO update rule to decrease the objective:

$$-\hat{\mathbb{E}}_{\mathcal{D}_i}[f_{\phi_{i+1}}^*(T_{\omega_{i+1}}(s, a))] - \mathcal{H}(\pi_{\theta_i}).$$
 - 7: **end for**
-

3.2 Enforcing f_ϕ^* Network to Represent the f -Divergence Space

The architecture of the f_ϕ^* network is crucial to obtain a family of convex conjugate generator functions f^* that represents the entire f -divergence space. To achieve this goal, two constraints need to be guaranteed (as discussed in Sec 3.2), including i) the **convexity constraint**, i.e., $f^*(u)$ is convex, and ii) the **zero gap constraint**, i.e., $\inf_{u \in \text{dom}_{f^*}} \{f^*(u) - u\} = 0$. To enforce the convex constraint,

we implement the f_ϕ^* network with a neural network structure convex to its input. Moreover, in each epoch, we estimate the minimum gap of $\delta = \inf_{u \in \text{dom}_{f^*}} \{f^*(u) - u\}$, with which we shift it to enforce the zero gap constraint. Below, we detail the design of the f_ϕ^* network.

1. Convexity constraint on f_ϕ^* network. The f_ϕ^* network takes a scalar input u from the reward signal network T_ω output, i.e., $u = T_\omega(s, a)$, with (s, a) as a state-action pair generated by π_θ . To ensure the convexity of the f_ϕ^* network, we employ the structure of a fully input convex neural network (FICNN) [3] with a composition of convex nonlinearities (e.g., ReLU) and linear mappings (See Fig. 2). The convex structure consists of multiple layer perceptrons. Differing from a fully connected feedforward structure, it includes shortcuts from the input layer u to all subsequent layers, i.e., for each layer $i = 0, \dots, k-1$,

$$z_{i+1} = g_i(W_i^{(z)} z_i + W_i^{(u)} z_0 + b_i), \quad \text{with} \quad f_\phi^*(u) = z_k + b_s \quad \text{and} \quad z_0 = u + b_s, \quad (6)$$

where z_i denotes the i -th layer activation, g_i represents non-linear activation functions, with $W_0^{(z)} \equiv 0$. b_s is a bias over both the input u and the last layer output z_k , which is used to enforce the zero gap constraint (as detailed below). As a result, the parameters in f_ϕ^* include $\phi = \{W_{0:k-1}^{(u)}, W_{1:k-1}^{(z)}, b_{0:k-1}, b_s\}$. Restricting $W_{1:k-1}^{(z)}$ to be non-negative and g_i 's to be convex non-decreasing activation functions (e.g. ReLU) guarantee the network output to be convex to the input $u = T_\omega(s, a)$. The convexity follows the fact that a non-negative sum of convex functions is convex and that the composition of a convex and convex non-decreasing function is also convex [9]. To ensure the non-negativity on $W_{1:k-1}^{(z)}$, in the training process, we clip the $W_{1:k-1}^{(z)}$ to be at least 0, i.e., $w = \max\{0, w\}$ for $\forall w \in W_{1:k-1}^{(z)}$, after each update to ϕ .

2. Zero gap constraint on f_ϕ^* network, i.e., $\inf_{u \in \text{dom}_{f^*}} \{f_\phi^*(u) - u\} = 0$. This constraint requires $f_\phi^*(u) \geq u$ for $\forall u \in \text{dom}_{f_\phi^*}$, with the equality attained. For a general convex function $f_\phi^*(u)$, its gap from u , defined as $\delta = \inf_{u \in \text{dom}_{f_\phi^*}} \{f_\phi^*(u) - u\}$, is not necessarily zero. We enforce the zero gap constraint by estimating δ and shifting $f_\phi^*(u)$ based on δ in each training epoch. We directly estimate the minimum gap δ by gradient descent with respect to u . Using δ , we shift $f_\phi^*(u)$ as follows,

$$f_{\phi'}^*(u) = f_\phi^*(u - \frac{\delta}{2}) - \frac{\delta}{2}, \quad \text{where} \quad \delta = \inf_{u \in \text{dom}_{f_\phi^*}} \{f_\phi^*(u) - u\}. \quad (7)$$

This shift guarantees zero gap constraint, and we delegate the proof to Appendix A. In each epoch, the estimation process of δ is detailed in Alg. 2, and the shift operation is implemented by updating $b'_s = b_s - \delta/2$. Fig. 3 illustrates the operations of estimating δ and shifting f_ϕ^* . Note that δ represents the minimum gap in function value between $f_\phi^*(u)$ and u . Shifting $\delta/2$ over both input and output space of $f_\phi^*(u)$ (i.e., Line 5 in Alg. 1) enforces the zero gap constraint. Note that this shifting operation is also performed, when initializing the parameters ϕ_0 for $f_\phi^*(u)$, to make sure the training starts from a valid f -divergence³.

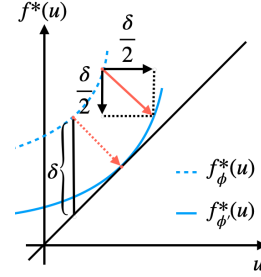


Figure 3: Illustration of shifting f_ϕ^* .

Algorithm 2 δ Estimation

Require: f_ϕ^* network; initial u_0 ; $\eta > 0$.

Ensure: δ .

- 1: **for** $i = 1, 2, \dots$ **do**
 - 2: $h = \nabla_u f_\phi^*(u) - 1$;
 - 3: $u_i = u_{i-1} - \eta \cdot h$;
 - 4: **end for**
 - 5: $\delta = f_\phi^*(u_i) - u_i$.
-

4 Experiments

We evaluate Alg. 1 by comparing it with baselines on six physical-based control tasks, including the CartPole [8] from the classic RL literature, and five complex tasks simulated with MuJoCo [32], such as HalfCheetah, Hopper, Reacher, Walker, and Humanoid. By conducting experiments on these tasks,

³Theoretically, given δ (defined as an infimum), it may not be achievable with a feasible $u \in \text{dom}_{f_\phi^*}$. However, empirically, given the diverse input distributions of f^* (See Sec 4.1), we can always introduce a projection operator [9] to limit the feasible space of u for a better control of the shift operation. In our experiments, we never found any issue when directly applying Alg. 2 for the shifting operation.

we show that *i)* our f -GAIL algorithm can learn diverse f -divergences, comparing to the limited choices in the literature (See Sec 4.1); *ii)* f -GAIL algorithm always learn policies performing better than baselines (See Sec 4.2); *iii)* f -GAIL algorithm is robust in performance with respect to structure changes in the f_ϕ^* network (See Sec 4.3).

Each task in the experiment comes with a true reward function, defined in the OpenAI Gym [10]. We first use these true reward functions to train expert policies with trust region policy optimization (TRPO) [29]. The trained expert policies are then utilized to generate expert demonstrations. To evaluate the data efficiency of f -GAIL algorithm, we sampled datasets of varying trajectory counts from the expert policies, while each trajectory consists of about 50 state-action pairs. Below are five IL baselines, we implemented to compare against f -GAIL.

- *Behavior cloning (BC)* [26]: A set of expert state-action pairs is split into 70% training data and 30% validation data. The policy is trained with supervised learning. BC can be viewed as minimizing KL divergence between expert’s and learner’s policies [20, 14].
- *Generative adversarial imitation learning (GAIL)* [18]: GAIL is an IL method using GAN architecture [15], that minimizes JS divergence between expert’s and learner’s behavior distributions.
- *BC initialized GAIL (BC+GAIL)*: As discussed in GAIL [18], BC initialized GAIL will help boost GAIL performance. We pre-train a policy with BC and use it as initial parameters to train GAIL.
- *Adversarial inverse reinforcement learning (AIRL)* [13]: AIRL applies the adversarial training approach to recover the reward function and its policy at the same time, which is equivalent to minimizing the reverse KL (RKL) divergence of state-action visitation frequencies between the expert and the learner [14].
- *Reverse KL - variational imitation (RKL-VIM)* [20]: the algorithm uses the RKL divergence instead of the JS divergence to quantify the divergence between expert and learner in GAIL architecture⁴.

For fair comparisons, the policy network structures π_θ of all the baselines and f -GAIL are the same in all experiments, with two hidden layers of 100 units each, and tanh nonlinearities in between. The implementations of reward signal networks and discriminators vary according to baseline architectures, and we delegate these implementation details to Appendix B. All networks were always initialized randomly at the start of each trial. For each task, we gave GAIL, BC+GAIL, AIRL, RKL-VIM and f -GAIL exactly the same amount of environment interactions for training.

4.1 f_ϕ^* Learned from f -GAIL

Fig. 4 shows that f -GAIL learned unique $f_\phi^*(u)$ functions for all six tasks, and they are different from those well-known divergences, such as RKL and JS divergences. Clearly, the learned $f_\phi^*(u)$ ’s are convex and with zero gap from u , thus represent valid f -divergences. Moreover, *the learned f -divergences are similar, when the underlying tasks share commonalities*. For example, the two $f_\phi^*(u)$ functions learned from CartPole and Reacher tasks (Fig. 4(a) and (d)) are similar, because the two tasks are similar, i.e., both aiming to keep a balanced distance from the controlling agent to a target. On the other hand, both Hopper and Walker tasks aim to train the agents (with one foot for Hopper and two feet for Walker) to proceed as fast as possible, thus their learned $f_\phi^*(u)$ are similar (Fig. 4(c) and (e)). (See Appendix B for descriptions and screenshots of tasks.) We also plot Fig. 5 to show that given a task, the learned f^* functions are consistent (small variance) for different sample sizes. Similar observations are made for tasks CartPole, Reacher and Humanoid as well.

In state-of-the-art IL approaches and our f -GAIL (from eq. (3) and (5)), the f^* -function takes the learner reward signal $u = T_\omega(s, a)$ (over generated state-action pairs (s, a) ’s) as input. By examining the distribution of u , two criteria can indicate that the learner policy π_θ is close to the expert π_E :

- u centers around zero gap*, i.e., $f^*(u) - u \approx 0$. This corresponds to the generator function f centered around $f(p(s, a)/q(s, a)) \approx f(1) = 0$, with p and q as the expert vs learner distributions;
- u has small standard deviation*. This means that u concentrates on the nearby range of zero gap, leading to a small f -divergence between learner and expert, since $D_f(p(s, a)||q(s, a)) \approx \int q(s, a)f(1)d(s, a) = 0$.

⁴Both AIRL and RKL-VIM can be viewed as RKL divergence minimization problem. However, they use different lower bounds on RKL divergence (See details in [14] and [20, 25]).

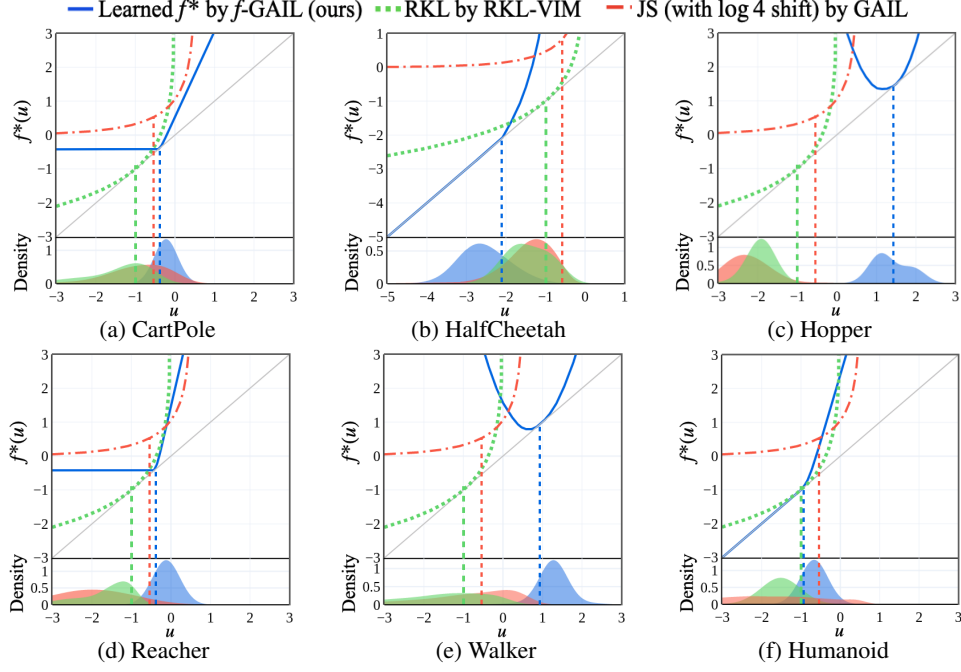


Figure 4: The learned $f_\phi^*(u)$ functions match the empirical input distributions at the zero gap regions with $f_\phi^*(u) - u \approx 0$, equivalently, $f(p(s,a)/q(s,a)) \approx f(1) = 0$, with close expert vs learner behavior distributions (i.e., p vs q). The distributions of input u were estimated by kernel density estimation [31] with Gaussian kernel of bandwidth 0.3.

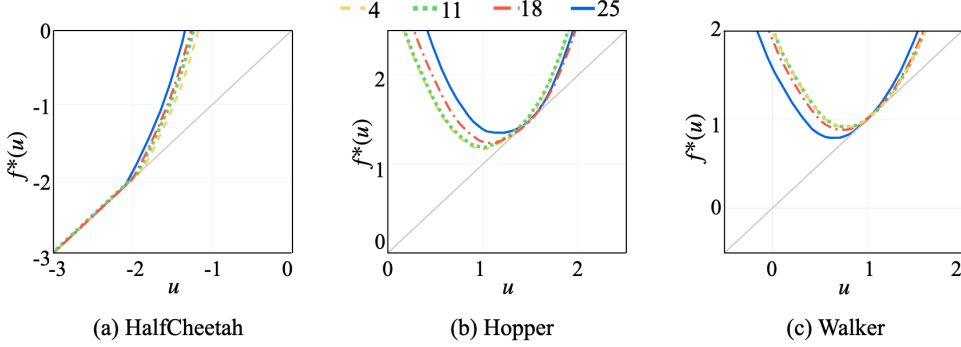


Figure 5: The learned $f_\phi^*(u)$ with different sample sizes.

In Fig. 4, we empirically estimated and showed the distributions of input u for the state-of-the-art IL methods (including GAIL and RKL-VIM⁵) and our f -GAIL. Fig. 4 shows that overall u distributions from our f -GAIL match the two criteria (i.e., close to zero gap and small standard deviation) better than baselines (See more statistical analysis on the two criteria across different approaches in Appendix B). This indicates that learner policies learned from f -GAIL are with smaller divergence, i.e., higher quality. We will provide experimental results on the learned policies to further validate this in Sec 4.2 below.

4.2 f -GAIL Performance in Policy Recovery

Fig. 6 shows the performances of our f -GAIL and all baselines under different training data sizes, and the tables in Appendix B provide detailed performance scores. In all tasks, our f -GAIL outperforms all the baselines. Especially, in more complex tasks, such as Hopper, Reacher, Walker, and Humanoid, f -GAIL shows a larger winning margin over the baselines, with at least 80% of expert performances for all datasets. GAIL shows lower performances on complex tasks such as Hopper, Reacher, Walker, and Humanoid, comparing to simple tasks, i.e., CartPole and

⁵With AIRL, similar results were obtained as that of RKL-VIM, since they both employ RKL divergence (while using different lower bounds). We omitted the results for AIRL for brevity.

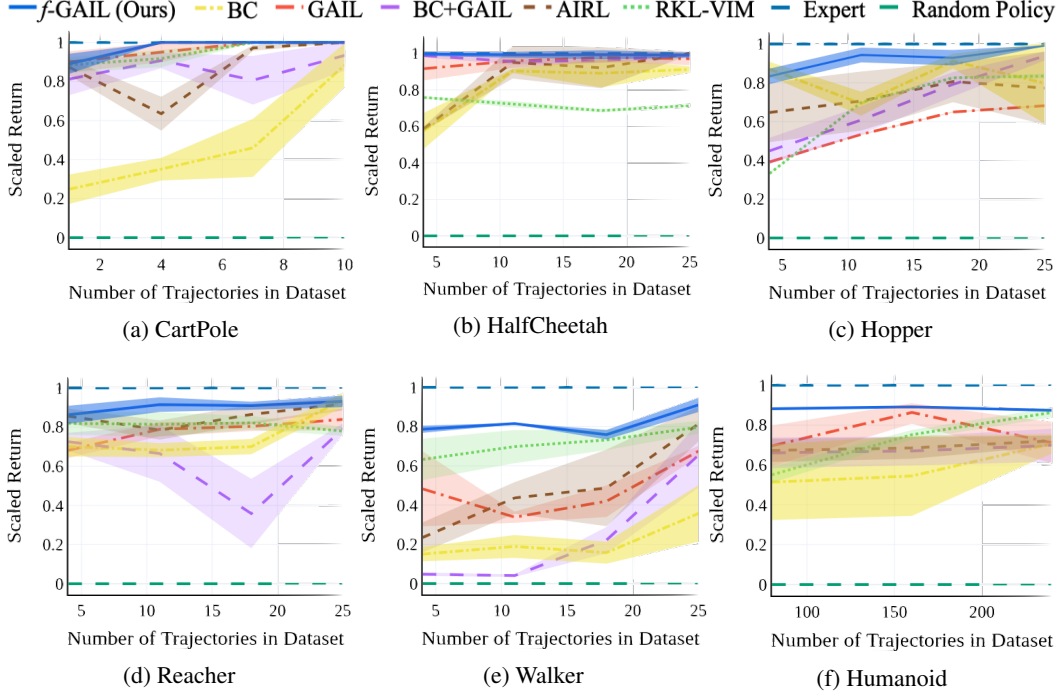


Figure 6: Performance of learned policies. The y -axis is the expected return (i.e., total reward), scaled so that the *expert* achieves 1 and a *random policy* achieves 0.

HalfCheetah (with much smaller state and action spaces). Overall, BC and BC initialized GAIL (BC+GAIL) have the lowest performances comparing to other baselines and our f -GAIL in all tasks. Moreover, they suffer from data efficiency problem, with extremely low performance when datasets are not sufficiently large. These results are consistent with that of [19], and the poor performances can be explained as a result of compounding error by covariate shift [27, 28]. AIRL performs poorly for Walker, with only 20% of expert performance when 4 trajectories were used for training, which increased up to 80% when using 25 trajectories. RKL-VIM had reasonable performances on CartPole, Hopper, Reacher, and Humanoid when sufficient amount of data was used, but was not able to get more than 80% expert performance for HalfCheetah, where our f -GAIL achieved expert performance. (See Tab. 6 in Appendix B for more detailed return values.) In terms of the convergence of the proposed f -GAIL, Fig. 7 below shows the training curve of f -divergence (i.e., the objective in eq. (5)) with respect to training epochs where it converges to less than 0.02 for HalfCheetah after 450 epochs. Similar results were observed in other tasks.

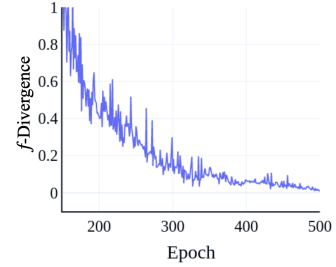


Figure 7: f -divergence curve in HalfCheetah.

4.3 Ablation Experiments

In this section, we investigate how structure choices of the proposed f^*_ϕ network, especially, the network expressiveness such as *the number of layers* and *the number of nodes per layer*, affect the model performance. In experiments, we took the CartPole, HalfCheetah and Reacher tasks as examples, and fixed the network structures of policy π_θ and the reward signal T_ω . We changed the number of layers to be 1, 2, 4, and 7 (with 100 nodes each layer) and changed the number of nodes per layer to be 25, 50, 100 and 200 (with 4 layers). The comparison results are presented in Tab. 2. In simpler tasks with smaller state and action space, e.g. the CartPole, we observed quick convergence with f -GAIL, achieving expert return of 200. In this case, the structure choices do not have impact on the performance. However, in more complex tasks such as HalfCheetah and Reacher, a simple linear transformation of input (with one convex transformation layer) is not sufficient to learn a good policy function π_θ . This naturally explains the better performances with the number of layers increased to 4 and the number of nodes per layer increased to 100. However, further increasing the number of layers to 7 and the number of nodes per layer to 200 decreased the performance a little bit. As a result, for

Table 2: Performances when changing *number of layers* and *number of nodes per layer* in f_ϕ^* network (Scores represent rewards. Higher scores indicate better learner policies).

Task	Number of Layers (100 nodes per layer)				Number of Nodes per Layer (4 layers)			
	1	2	4	7	25	50	100	200
HalfCheetah	1539±144	4320± 81	4445±79	4100 ± 51	3546±132	4058± 127	4445±79	4343 ± 80
Reacher	-22.8± 4.2	-16.4± 3.2	-10.6±2.6	-15.8±2.8	-25.2± 5.35	-14.1 ± 5.2	-10.6±2.6	-12.6±4.0
CartPole		200±0				200±0		

these tasks, 4 layers with each layer of 100 nodes suffice to represent an f^* -function. Consistent observations were made in other tasks, and we omit those results for brevity.

5 Discussion and Future Work

Our work makes the first attempt to model imitation learning with a learnable f -divergence from the underlying expert demonstrations. The model automatically learns an f -divergence between expert and learner behaviors, and a policy that produces expert-like behaviors.

Meaning of the best f -divergence. As a minimax optimization problem in eq. (5), f -GAIL searches for the best f -divergence in the “max” inner-loop *given the current learned policy* π learned from the “min” outer-loop, eventually leading to a stable solution of (π, f^*) . Here, given an expert demonstration dataset, a better divergence can measure the discrepancy more precisely than other divergences, thus enables training a learner with closer behaviors to the expert.

Future work. This work focuses on searching within the f -divergence space, where Wasserstein distance [17, 4] is not included. However, the divergence search space can be further extended to c -Wasserstein distance family [2], which subsumes f -divergence family and Wasserstein distance as special cases. Designing a network structure to represent c -Wasserstein distance family is challenging (we leave it as part of our future work), while a naive way is to model it as a convex combination of the f -divergence family (using our f_ϕ^* network) and Wasserstein distance. Moreover, beyond imitation learning, our f^* -network structure can be potentially “coupled” with f -GAN [25] and f -EBM [33] to learn an f -divergence between the generated vs real data distributions (e.g., image and audio files), which in turn trains a higher quality generator.

Broader Impact

This paper aims to advance the imitation learning techniques, by learning an optimal discrepancy measure from f -divergence family, which has a wide range of applications in robotic engineering, system automation and control, etc. The authors do not expect the work will address or introduce any societal or ethical issues.

Acknowledgments and Disclosure of Funding

Xin Zhang and Yanhua Li were supported in part by NSF grants IIS-1942680 (CAREER), CNS-1952085, CMMI-1831140, and DGE-2021871. Ziming Zhang was supported in part by NSF CCF-2006738. Zhi-Li Zhang was supported in part by NSF grants CMMI-1831140 and CNS-1901103.

References

- [1] Pieter Abbeel and Andrew Y Ng. Apprenticeship learning via inverse reinforcement learning. In *Proceedings of the twenty-first international conference on Machine learning*, page 1. ACM, 2004.
- [2] Luca Ambrogioni, Umut Güçlü, Yağmur Güçlütürk, Max Hinne, Marcel AJ van Gerven, and Eric Maris. Wasserstein variational inference. In *Advances in Neural Information Processing Systems*, pages 2473–2482, 2018.

- [3] Brandon Amos, Lei Xu, and J Zico Kolter. Input convex neural networks. In *Proceedings of the 34th International Conference on Machine Learning-Volume 70*, pages 146–155. JMLR. org, 2017.
- [4] Martin Arjovsky, Soumith Chintala, and Léon Bottou. Wasserstein gan. *arXiv preprint arXiv:1701.07875*, 2017.
- [5] Dilip Arumugam, Debadeepta Dey, Alekh Agarwal, Asli Celikyilmaz, Elnaz Nouri, Eric Horvitz, and Bill Dolan. Reparameterized variational divergence minimization for stable imitation. 2019.
- [6] Christopher G Atkeson and Stefan Schaal. Robot learning from demonstration. In *ICML*, volume 97, pages 12–20. Citeseer, 1997.
- [7] Andrew R Barron, Lhszl Györfi, and Edward C van der Meulen. Distribution estimation consistent in total variation and in two types of information divergence. *IEEE transactions on Information Theory*, 38(5):1437–1454, 1992.
- [8] Andrew G Barto, Richard S Sutton, and Charles W Anderson. Neuronlike adaptive elements that can solve difficult learning control problems. *IEEE transactions on systems, man, and cybernetics*, (5):834–846, 1983.
- [9] Stephen Boyd, Stephen P Boyd, and Lieven Vandenberghe. *Convex optimization*. Cambridge university press, 2004.
- [10] Greg Brockman, Vicki Cheung, Ludwig Pettersson, Jonas Schneider, John Schulman, Jie Tang, and Wojciech Zaremba. Openai gym. *arXiv preprint arXiv:1606.01540*, 2016.
- [11] Imre Csiszár, Paul C Shields, et al. Information theory and statistics: A tutorial. *Foundations and Trends® in Communications and Information Theory*, 1(4):417–528, 2004.
- [12] Chelsea Finn, Paul Christiano, Pieter Abbeel, and Sergey Levine. A connection between generative adversarial networks, inverse reinforcement learning, and energy-based models. *arXiv preprint arXiv:1611.03852*, 2016.
- [13] Justin Fu, Katie Luo, and Sergey Levine. Learning robust rewards with adversarial inverse reinforcement learning. *arXiv preprint arXiv:1710.11248*, 2017.
- [14] Seyed Ghasemipour, Richard Zemel, and Shixiang Gu. A divergence minimization perspective on imitation learning methods. *arXiv preprint arXiv:1911.02256*, 2019.
- [15] Ian Goodfellow, Jean Pouget-Abadie, Mehdi Mirza, Bing Xu, David Warde-Farley, Sherjil Ozair, Aaron Courville, and Yoshua Bengio. Generative adversarial nets. In *Advances in neural information processing systems*, pages 2672–2680, 2014.
- [16] Jean-Baptiste Hiriart-Urruty and Claude Lemaréchal. *Fundamentals of convex analysis*. Springer Science & Business Media, 2012.
- [17] Frank L Hitchcock. The distribution of a product from several sources to numerous localities. *Journal of mathematics and physics*, 20(1-4):224–230, 1941.
- [18] Jonathan Ho and Stefano Ermon. Generative adversarial imitation learning. In *Advances in Neural Information Processing Systems*, pages 4565–4573, 2016.
- [19] Rohit Jena and Katia Sycara. Loss-annealed gail for sample efficient and stable imitation learning. *arXiv preprint arXiv:2001.07798*, 2020.
- [20] Liyiming Ke, Matt Barnes, Wen Sun, Gilwoo Lee, Sanjiban Choudhury, and Siddhartha Srinivasa. Imitation learning as f -divergence minimization. *arXiv preprint arXiv:1905.12888*, 2019.
- [21] Diederik P Kingma and Jimmy Ba. Adam: A method for stochastic optimization. *arXiv preprint arXiv:1412.6980*, 2014.
- [22] Solomon Kullback and Richard A Leibler. On information and sufficiency. *The annals of mathematical statistics*, 22(1):79–86, 1951.
- [23] Friedrich Liese and Igor Vajda. On divergences and informations in statistics and information theory. *IEEE Transactions on Information Theory*, 52(10):4394–4412, 2006.
- [24] Jianhua Lin. Divergence measures based on the shannon entropy. *IEEE Transactions on Information theory*, 37(1):145–151, 1991.

- [25] Sebastian Nowozin, Botond Cseke, and Ryota Tomioka. f-gan: Training generative neural samplers using variational divergence minimization. In *Advances in neural information processing systems*, pages 271–279, 2016.
- [26] Dean A Pomerleau. Efficient training of artificial neural networks for autonomous navigation. *Neural Computation*, 3(1):88–97, 1991.
- [27] Stéphane Ross and Drew Bagnell. Efficient reductions for imitation learning. In *Proceedings of the thirteenth international conference on artificial intelligence and statistics*, pages 661–668, 2010.
- [28] Stéphane Ross, Geoffrey Gordon, and Drew Bagnell. A reduction of imitation learning and structured prediction to no-regret online learning. In *Proceedings of the fourteenth international conference on artificial intelligence and statistics*, pages 627–635, 2011.
- [29] John Schulman, Sergey Levine, Pieter Abbeel, Michael Jordan, and Philipp Moritz. Trust region policy optimization. In *International conference on machine learning*, pages 1889–1897, 2015.
- [30] John Schulman, Philipp Moritz, Sergey Levine, Michael Jordan, and Pieter Abbeel. High-dimensional continuous control using generalized advantage estimation. *arXiv preprint arXiv:1506.02438*, 2015.
- [31] Simon J Sheather and Michael C Jones. A reliable data-based bandwidth selection method for kernel density estimation. *Journal of the Royal Statistical Society: Series B (Methodological)*, 53(3):683–690, 1991.
- [32] Emanuel Todorov, Tom Erez, and Yuval Tassa. Mujoco: A physics engine for model-based control. In *2012 IEEE/RSJ International Conference on Intelligent Robots and Systems*, pages 5026–5033. IEEE, 2012.
- [33] Lantao Yu, Yang Song, Jiaming Song, and Stefano Ermon. Training deep energy-based models with f-divergence minimization. 2020.

A Proof for Equation (7) in Section 3.2

In Section 3.2, we propose a shifting operation in eq. (7) to transform any convex function to a convex conjugate generator function of an f -divergence. Below, we summarize the shifting operation and prove its efficacy in proposition A.1.

Proposition A.1. *Given a convex function $f_\phi^* : \text{dom}_{f_\phi^*} \mapsto \mathbb{R}$, applying the shifting operation below transforms it to a convex conjugate generator function of an f -divergence,*

$$f_{\phi'}^*(u) = f_\phi^*\left(u - \frac{\delta}{2}\right) - \frac{\delta}{2}, \quad \text{where } \delta = \inf_{u \in \text{dom}_{f_\phi^*}} \{f_\phi^*(u) - u\}. \quad (8)$$

Proof. As presented in Section 3.2, for an f -divergence, its convex conjugate generator function $f_{\phi'}^*(u)$ is *i)* convex, and *ii)* with zero gap from u , i.e., $\inf_{u \in \text{dom}_{f_{\phi'}^*}} \{f_{\phi'}^*(u) - u\} = 0$. Below, we prove that both these two constraints hold for the obtained $f_{\phi'}^*(u)$.

Convexity. Since a constant shift of a convex function preserves the convexity [9], the obtained $f_{\phi'}^*(u)$ is convex.

Zero gap. Given $\delta = \inf_{u \in \text{dom}_{f_\phi^*}} \{f_\phi^*(u) - u\}$, we denote the \tilde{u} as the value that attains the infimum. Hence, we have $f_\phi^*(u) - u \geq \delta$ for $\forall u \in \text{dom}_{f_\phi^*}$. For the transformed function $f_{\phi'}^*(u) = f_\phi^*\left(u - \frac{\delta}{2}\right) - \frac{\delta}{2}$, we naturally have

$$f_{\phi'}^*(u) - u = f_\phi^*\left(u - \frac{\delta}{2}\right) - \frac{\delta}{2} - u = f_\phi^*\left(u - \frac{\delta}{2}\right) - \left(u - \frac{\delta}{2}\right) - \delta \geq \delta - \delta = 0, \quad \forall u \in \text{dom}_{f_{\phi'}^*},$$

and the infimum is attained at $\tilde{u} + \frac{\delta}{2}$. This implies that the zero gap constraint $\inf_{u \in \text{dom}_{f_{\phi'}^*}} \{f_{\phi'}^*(u) - u\} = 0$ holds. □

B Environments and Detailed Results

The environments we used for our experiments are from the OpenAI Gym [10] including the CartPole [8] from the classic RL literature, and five complex tasks simulated with MuJoCo [32], such as HalfCheetah, Hopper, Reacher, Walker, and Humanoid with task screenshots and version numbers shown in Fig. 8.

Details of policy network structures. The policy network structures π_θ of all the baselines and f -GAIL are the same in all experiments, with two hidden layers of 100 units each, and tanh nonlinearities in between. Note that behavior cloning (BC) employs the same structure to train a policy network with supervised learning.

Details of reward signal network structures. The reward signal network used in GAIL, BC+GAIL, AIRL, RKL-VIM and f -GAIL are all composed of three hidden layers of 100 units each with first two layers activated with tanh, and the final activation layers listed in Tab. 3.

Details of f_ϕ^* network structure in f -GAIL. For the study of the f^* function in Sec 4.1 and the performances of the learned policy in Sec 4.2, the f_ϕ^* network is composed of 4 linear layers with hidden layer dimension of 100 and ReLU activation in between. For the ablation study in Sec 4.3, we changed the number of linear layers to be 1, 2, 4 and 7 (with 100 nodes per layer) and the number of nodes per layer to be 25, 50, 100, and 200 (with 4 layers).

Evaluation setup. For all the experiments, the amount of environment interaction used for GAIL, BC+GAIL, AIRL, RKL-VIM and the f -GAIL together with expert and random policy performances in each task is shown in Tab. 4. We followed GAIL [18] to fit value functions, with the same neural network architecture as the policy networks, and employed generalized advantage estimation [30] with $\gamma = 0.99$ and $\lambda = 0.95$, so that the gradient variance is reduced.

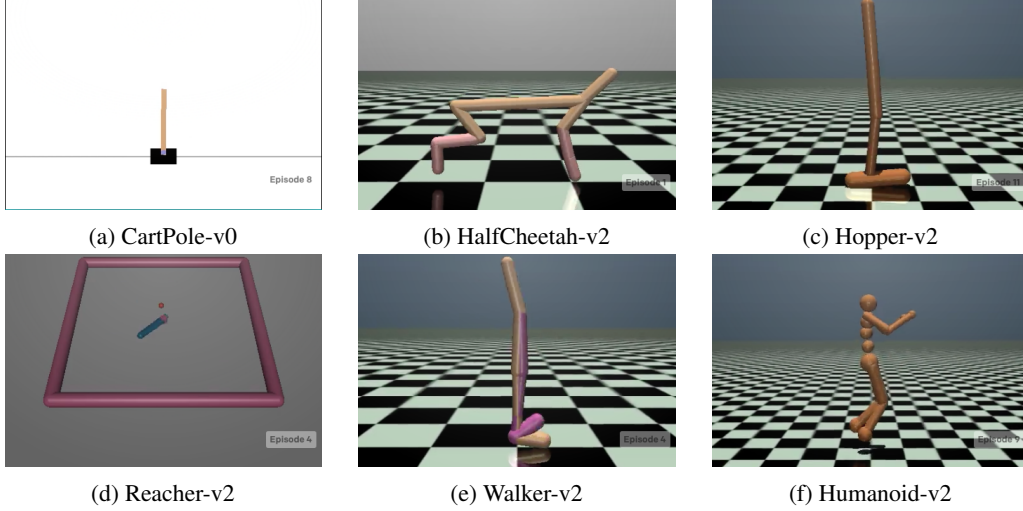


Figure 8: Screenshots of six physics-based control tasks [32].

Table 3: Final layer activation functions for Reward Signal Networks.

IL methods	Activation
GAIL	$\text{Sigmoid}(v)$
BC+GAIL	$\text{Sigmoid}(v)$
AIRL	$\text{Sigmoid}(v)$
RKL-VIM	$-\exp(v)$

Table 4: Parameters for baselines and f -GAIL.

Task	Training Number of (s, a)		Expert performance	Random policy performance
	iterations	per iteration		
CartPole-v0	200	200	200 ± 0	17 ± 4
HalfCheetah-v2	500	2000	4501 ± 118	-901 ± 49
Hopper-v2	500	2000	3593 ± 19	8 ± 6
Reacher-v2	500	2000	-4.5 ± 1.7	-93.7 ± 4.8
Walker-v2	500	2000	5657 ± 33	-2 ± 3
Humanoid-v2	700	30000	10400 ± 55	101 ± 26

B.1 Detailed statistical results on Learned f_ϕ^* function

As explained in Sec 4.1, two criteria for the input distribution to the f_ϕ^* function govern the quality of the learned policy π_θ , namely, (i) input u centers around zero gap; (ii) input u has small standard deviation. Now, based on Fig. 4, we analyze how much different IL methods satisfy the two criteria in all six tasks.

- To quantify criterion (i), we denote \tilde{u} as the input value with zero gap, i.e., $f_\phi^*(\tilde{u}) - \tilde{u} = 0$, and \bar{u} as the mean of the input u . Thus, we quantify the criterion (i) using the absolute difference between \tilde{u} and \bar{u} , i.e., $\Delta_u = |\tilde{u} - \bar{u}|$.
- To quantify criterion (ii), we estimate the standard deviations σ of input distributions for different IL methods in all tasks.

For both Δ_u and σ , the smaller values indicate a learner policy closer to expert policy. As a result, we examine their sum, i.e., $\Delta_u + \sigma$ as a unifying metric to evaluate overall how the two criteria are met. Tab. 5 shows the detailed results of Δ_u , σ , and $\Delta_u + \sigma$. It shows that our proposed f -GAIL learns an f_ϕ^* function with consistently lower values on $\Delta_u + \sigma$, comparing to all baselines, which indicates that the learned f_ϕ^* function from f -GAIL can meet the two criteria better than baselines.

B.2 Detailed results on learner policies

The exact learned policy return are listed in Tab. 6. The means and standard deviations are computed over 50 trajectories. A higher return indicates a better learned policy. All results are computed over 5 policies learned from random initializations.

Table 5: Analysis on input distributions of f^* functions.

Task	CartPole	HalfCheetah	Hopper	Reacher	Walker	Humanoid
f -GAIL	0.28	0.62	0.51	0.60	0.49	0.52
RKL-VIM	1.25	0.96	1.36	2.14	4.62	2.85
GAIL	1.96	1.31	2.09	2.08	4.06	3.55

Table 6: Learned policy performance.

Task	Datasize	BC	GAIL	BC+GAIL	AIRL	RKL-VIM f -GAIL (Ours)	
CartPole	1	62±13	181±9	165±14	176±7	179±7	180±9
	4	81±10	191±9	183±7	133±15	185±8	200±0
	7	101±27	200±0	164±22	194±2	200±0	200±0
	10	178±20	199±0	187±13	200±0	200±0	200±0
HalfCheetah	4	2211±528	4047±344	4431±56	2276±65	3194±30	4481±60
	11	3979±61	4274±202	4263±90	4230±473	2994±94	4457±89
	18	3911±416	4377±135	4282±67	4073±605	2806±46	4461±132
	25	4027±91	4340±185	4447±48	4501±42	2952±45	4445±79
Hopper	4	3129±132	1413±26	1619±240	2328±549	1200±16	2996±142
	11	2491±218	1923±16	2188±257	2539±544	2513±3	3390±135
	18	3276±133	2336±10	2849±224	2898±362	2969±17	3339±142
	25	2868±745	2452±12	3372±79	2779±675	3001±42	3561±6
Reacher	4	-31.3±4.4	-33.0± 3.5	-29.0±4.0	-17.4±3.3	-20.7±5.2	-16.7±4.0
	11	-32.9±3.1	-23.4± 3.2	-34.4±12.8	-23.7±4.3	-21.1±5.4	-12.1±3.3
	18	-31.3±3.4	-22.1± 2.1	-61.8±15.7	-16.6±4.4	-20.4±3.1	-12.6±1.8
	25	-10.0±3.2	-18.9± 5.0	-23.2±2.4	-11.8±2.9	-24.2±2.0	-10.6±2.6
Walker2d	4	848±206	2728±1079	267±50	1327±431	3577±594	4448±103
	11	1068±328	1911±160	226±36	2466±454	3947±475	4609±22
	18	888±316	2372±453	1251±378	2755±1103	4138±287	4290±139
	25	2018±812	3816±148	3700±939	4599±504	4507±179	5148±205
Humanoid	80	5391±3918	7268±2101	6908±1577	7034±591	5772±409	9180±49
	160	5713±4126	8994±1053	7003±1488	7160±559	7842±245	9280±68
	240	7378±998	7430±2106	7294±1705	7528±273	8993±252	9130±114